Broadband matched-field processing of transient signals in shallow water

S. M. Jesus[a)]
SACLANT Undersea Research Centre, Viale San Bartolomeo 400, I-19138 La Spezia, Italy

(Received 22 January 1992; revised 13 April 1992; accepted 18 November 1992)

Range and depth source localization in shallow water amounts to the estimation of the normal-mode structure of the acoustic field. As "seen" by a vertical array, and from a modeling point of view, the normal-mode structure appears as a set of nonplane coherent waves closely spaced at a vertical angle. This paper presents a full-wave-field narrow-band high-resolution technique that uses the spectral decomposition of the sample covariance matrix to resolve the vertical arrival structure of the harmonic acoustic field. The broadband processor is obtained by weighted averaging of the narrow-band range-depth ambiguity estimates within the source signal frequency band. Results obtained on synthetic data show that its performance is always better than or equal to that of the generalized minimum variance processor, which itself largely outperforms the conventional matched-field processor. It is shown, using both simulated and experimental data, that the effect of the broadband processor is to increase the stability of the source location estimate. Results obtained with this processor on short transient pulses collected during the North Elba'89 experiment with a 62-m-aperture vertical array, showed stable and accurate localizations over long time intervals. It is also shown that the sound field, received over a given frequency band, is relatively stable over time and is in agreement with the predictions given by a standard normal-mode propagation model.

PACS numbers: 43.30.Wi, 43.60.Gk, 43.60.Pt

INTRODUCTION

Matched-field processing of vertical arrays is now a well-known technique for range and depth localization of sound sources in the ocean. Following the pioneering work of Hinich[1] and Bucker[2] a large number of theoretical studies have been published that were aimed at comparing various matched-field processors and testing their robustness to erroneous and/or incomplete knowledge of environmental or system parameters.[3–15] Despite this large effort, reports of successful experimental results have been rare. References 11, 15–17 include some studies of experimental matched-field localization in shallow water. Results obtained in deep water can be found in Ref. 7 for an under-ice propagation environment and in Refs. 18,19 for typical Pacific environments. Most of the matched-field experiments that have been reported used a continuous wave (cw) sound source received on a vertical array of sensors spanning a significant part of the water column (except in Ozard[16] in which a sparse bottom moored array was used). At least three different narrow-band matched-field processors have been used on experimental data: the conventional matched-field processor,[11,15,18] the normal-mode matching processor,[7,15] and the generalized minimum variance processor.[17,18] Hodgkiss and Brienzo[19] used a broadband conventional matched-field processor in a deep water environment. In all the above-referenced literature, there is no evidence of stable source localization results and, in general, only occasional agreement was found between the measured and the predicted sound field; in most cases only a few (and sometimes only one) range-depth surfaces were shown for each data set.

This paper shows, using experimental data, that stable and accurate range-depth localization of a sound source in shallow water is possible by matched-field processing of a vertical array. This was achieved by extending the well-known narrow-band plane-wave MUSIC algorithm to full-wave-field broadband range-depth estimation. In particular, this paper demonstrates that a high-quality source location estimate can be obtained by the intersection between the replica acoustic vector continuum (propagation model prediction for all possible source locations) and a vector subspace of known dimension spanned by the normal modes significantly excited by the acoustic source(s) called *the mode subspace*. A broadband processor is then computed by weighted averaging of the narrow-band estimates over the frequency band of the source signal. It is shown, with both synthetic and experimental data, that the proposed broadband processor provides higher source localization stability than the narrow-band processor in the same conditions. The application of this technique to the localization of short transient pulses transmitted in a (assumed) range-independent waveguide of 120-m depth and received on a 62-m aperture vertical array showed that precise and stable results could be obtained during longer time intervals than those normally found in the literature.

I. THEORY

A. The data model

The received signal is modeled as the solution of the wave equation at the receiver location for a narrow-band

[a)] Actually at UCEH-University of Algarve, Campus de Gambelas, 8000 Faro, Portugal.

 0001-4966/93/041841-10$06.00

point source exciting a horizontally stratified, parallel waveguide. The normalized spatial dependence of the acoustic pressure field measured at a vertical array of L sensors due to a unit power harmonic source at location $\theta_T' = (z_T, r_T)$—where superscript $'$ stands for transpose and subscript $_T$ indicates the true source location—is commonly expressed as a linear combination of the waveguide normal-mode depth functions,[20] i.e.,

$$\mathbf{p}(\theta_T,\omega_k) = \mathbf{A}(\omega_k)\mathbf{x}(\theta_T,\omega_k), \tag{1}$$

where $\mathbf{p}(\theta_T,\omega_k)$ is the L-dimensional array output vector, $\mathbf{A}(\omega_k)$ is an $L \times M_k$ real matrix whose columns are the normal-mode depth functions expressed for all sensor depths $\{z_l; l = 1,...,L\}$, and M_k is the number of modes supported by the waveguide at frequency ω_k. The M_k-dimensional complex vector $\mathbf{x}(\theta_T,\omega_k)$ represents the model normal-mode structure at frequency ω_k and for the true source parameter location θ_T,

$$x_m(\theta_T,\omega_k) = \frac{a_m(z_T,\omega_k)}{\sqrt{k_m(\omega_k)}} \times \exp[-\alpha_m(\omega_k)r_T + ik_m(\omega_k)r_T], \tag{2}$$

where $\alpha_m(\omega_k)$ is the mth mode attenuation coefficient. The two sets $\{a_m(z,\omega_k); m = 1,...,M_k; 0 < z < H\}$ and $\{k_m(\omega_k); m = 1,...,M_k\}$ are the mode depth functions and the corresponding mode horizontal wave numbers characterizing the propagation channel of depth H at frequency ω_k. Note that (1) and (2) have been obtained by normalizing the range dependence, a phase shift, and an arbitrary constant. Let $\mathbf{y}(\theta_T, iT_s)$ be the L-dimensional array of received acoustic pressure at a discrete time iT_s where the sampling period T_s is chosen such that $T_s \leqslant 1/2f_{\max}$. The signal plus noise $\mathbf{y}(\theta_T, iT_s)$ is assumed to be stationary over the recording time interval T_r. This interval T_r is then segmented into N equal intervals with $2K$ samples each, $T_r = 2NKT_s$. On each of these intervals a fast Fourier transform (FFT) is then performed. Let

$$\mathbf{y}(\theta_T,\omega_k) = b_n(\omega_k)\mathbf{A}(\omega_k)\mathbf{x}(\theta_T,\omega_k) + \epsilon_n(\omega_k), \quad n = 1,...,N; \quad k = 1,...,K, \tag{3}$$

be, for a given k, an N sample draw of a multivariate, complex, normally distributed random variable Y, $N(\mathbf{0},\mathbf{R}_y)$ where the signal in Eq. (1) is assumed to be corrupted by additive, uncorrelated, and zero-mean complex Gaussian noise ϵ_n and where $b_n(\omega_k)$ is a complex random variable that represents the source amplitude at frequency ω_k and time snapshot n. At this point, the vector $\mathbf{x}$ may be considered either deterministic with $\Sigma_{\alpha=1}^{N}\mathbf{x}_\alpha = \mathbf{0}$ and $\Sigma_{\alpha=1}^{N}\mathbf{x}_\alpha\mathbf{x}_\alpha^H = \mathbf{R}_x$ or random with $E\{\mathbf{x}\} = \mathbf{0}$ and $E\{\mathbf{x}\mathbf{x}^H\} = \mathbf{R}_x$. In either case, and even if $\mathbf{A}$ is singular, Y is distributed as defined above with $\mathbf{R}_y = \mathbf{A}\mathbf{R}_x\mathbf{A}' + \mathbf{R}_\epsilon$ (Ref. 21). The method presented in this paper applies for $\mathbf{x}$ deterministic or random.

B. Conventional matched-field processing

The conventional range-depth source localization technique consists of passing the received acoustic pressure $\{\mathbf{y}_n(\theta_T,\omega_k); n = 1,...,N; k = 1,...,K\}$ through a bank of narrow-band matched filters based on the model replica prediction for each range-depth location θ, i.e.,

$$\mathrm{RD}_{\mathrm{CMF}}(\theta,\omega_k) = \mathbf{p}(\theta,\omega_k)^H\hat{\mathbf{R}}_y(\omega_k)\mathbf{p}(\theta,\omega_k), \quad \theta\in\Theta, \tag{4}$$

where Θ is the two-dimensional range-depth parameter search space and $\hat{\mathbf{R}}_y(\omega_k)$ is the sample cross-covariance matrix of the received signal, commonly estimated as the N sample mean of the received data outer product. The source location estimate $\hat{\theta}_T$ is obtained as the coordinates of the absolute maximum of the ambiguity surface given by (4).

C. The mode subspace approach

The mode subspace approach brings together the ideas of noise suppression and *a priori* model structure knowledge in order to enhance source detection in waveguide types of propagation. An efficient way of solving (3) for $\mathbf{x}(\theta_T,\omega_k)$ is by using the mapping of the data vector into the subspace spanned by the columns of matrix $\mathbf{A}(\omega_k)$ which is the mode subspace. The modal structure $\mathbf{x}(\theta_T,\omega_k)$ simply represents the coordinates of one point in that subspace. The intersection of the replica acoustic vector continuum $\{\mathbf{p}(\theta,\omega_k); \theta\in\Theta\}$ and the mode subspace will give the solution $\mathbf{x}(\theta_T,\omega_k)$ and thus θ_T. Assuming $L > M_k$, the subspace spanned by the eigenvectors of the sample cross-covariance matrix $\hat{\mathbf{R}}_y(\omega_k)$ associated with the largest M_k eigenvalues is the maximum likelihood estimate of the required mode subspace.[22] Therefore, defining the eigendecomposition of $\hat{\mathbf{R}}_y(\omega_k)$ as $\hat{\mathbf{R}}_y(\omega_k) = \hat{\mathbf{E}}(\omega_k)\hat{\Lambda}(\omega_k)\hat{\mathbf{E}}(\omega_k)^H$, the mode subspace span is

$$\hat{\mathbf{E}}_{M_k}(\omega_k) = [\hat{\mathbf{e}}_1,\hat{\mathbf{e}}_2,...,\hat{\mathbf{e}}_{M_k}], \tag{5}$$

with the corresponding eigenvalues, $\hat{\lambda}_1 \geqslant \hat{\lambda}_2 \geqslant,...,\geqslant \hat{\lambda}_{M_k}$. Finding the intersection between the mode subspace and the acoustic replica vector continuum $\{\mathbf{p}(\theta,\omega_k); \theta\in\Theta\}$ is equivalent to the minimization of the square distance[22]

$$d^2(\theta,\omega_k) = |\hat{\mathbf{E}}_{L-M_k}(\omega_k)\hat{\mathbf{E}}_{L-M_k}^H(\omega_k)\mathbf{p}(\theta,\omega_k)|^2, \quad \theta\in\Theta, \tag{6}$$

where $\hat{\mathbf{E}}_{L-M_k}(\omega_k)$ is the mode subspace orthogonal complement. Thus, the source location estimate $\hat{\theta}_T$ is given by the coordinates of the maximum of the multi-dimensional surface obtained by plotting the functional

$$\mathrm{RD}_{\mathrm{MS}}(\theta,\omega_k) = d^{-2}(\theta,\omega_k), \quad \theta\in\Theta. \tag{7}$$

The mode subspace approach is a full-wave-field generalization of the MUSIC algorithm commonly used in spatial array processing for directions-of-arrival (DOA) estimation.[22,23] This generalization was made possible due to the similarities on the structure of the assumed data model. However, there is at least one fundamental difference between the two approaches that concerns the estimation of the mode (or signal) subspace. In the MUSIC algorithm, the so-called signal subspace is spanned by the direction vectors of the, say P, sources contributing to the field. The estimation of the number P is generally achieved by means of a statistical test based on the whiteness of the noise field. The solution to this problem is known to be determinant for real

data applications: if the number P is underestimated some source directions may not be accounted for; if the number P is overestimated spurious sources may appear giving rise to false detections. In this paper it is suggested that the criterion for determining the dimension of the mode subspace should be based on the number of modes M_k supported by the waveguide at frequency ω_k. It is clear from (1) that the maximum dimension of the subspace spanned by the source signal spatial field received at the array is bounded by the rank of matrix $\mathbf{A}(\omega_k)$, i.e., at maximum M_k if $M_k < L$.

1. The monopulse case

The problem of cross-spectral matrix estimation from a single data snapshot represents our experimental data application situation (transient signals). In the case where the number of data snapshots N is small, $N < L$ and in particular if $N = 1$, the rank of the matrix is at maximum equal to N. The solution to the problem is always given by the intersection between the replica vector continuum and the M_k-dimensional mode subspace defined by (5). The cross-spectral matrix in that case is ill-conditioned and the $M_k - N$ smallest eigenvalues of the mode subspace may be very small, i.e., of the same order of those associated with the noise subspace.

2. The case $M_k > L$

This case manifests itself when a few-hydrophone array is used or, in a deep-water/high-frequency situation. In this case the solution is given by the largest dimensional signal subspace that can be reached with the given array, i.e., $\mathbf{E}_{L-1}$. The result is degraded because not all the modes can be resolved by the receiver. The amount of degradation depends on the effective contribution to the sound field of the modes that are left out of the mode subspace. As an example, the degradation due to a sparse array receiving a high-frequency signal propagating in a waveguide with a high attenuation bottom is small compared to the degradation found in the presence of a highly reflecting bottom. Note that this degradation is common to all the other matched-field processors.[11,15]

D. The broadband matched-field processor

The broadband matched-field processor is obtained by a weighted average of the range-depth ambiguity surfaces calculated for each narrow-band cell over the source signal bandwidth. Thus, if the source signal bandwidth is $[\omega_{k_1},\omega_{k_2}]$,

$$\mathrm{RD}_{[\cdot\,1]}(\theta) = \frac{1}{k_2 - k_1 + 1} \sum_{k=k_1}^{k_2} \beta_k \, \mathrm{RD}_{[\cdot\,1]}(\theta,\omega_k), \quad \theta \in \Theta, \tag{8}$$

where $\{\beta_k; k = k_1,\ldots,k_2\}$ is a weighting function. It can be shown that if the conventional matched-field processor (4) is used and the weighting function β_k is proportional to the source signal power spectrum, then (8) is the optimum range-depth receiver of the given source signal conditioned on the propagation model assumed in $\mathbf{p}(\theta,\omega_k)$. This type of processor has been used, under a different form in Ref. 19. In the case of the mode subspace processor, (7) is replaced in (8) and the final estimate is conditioned also on the normal-mode structure of the signal field.

II. SIMULATION PERFORMANCE EXAMPLE

The system/environment scenario shown in Fig. 1 was that of the SACLANTCEN North Elba'89 experiment that took place north of Elba Island (Italy) in Nov./Dec. 1989. The environmental parameters were established in Ref. 24. The SACLANTCEN normal-mode code (SNAP)[25] was

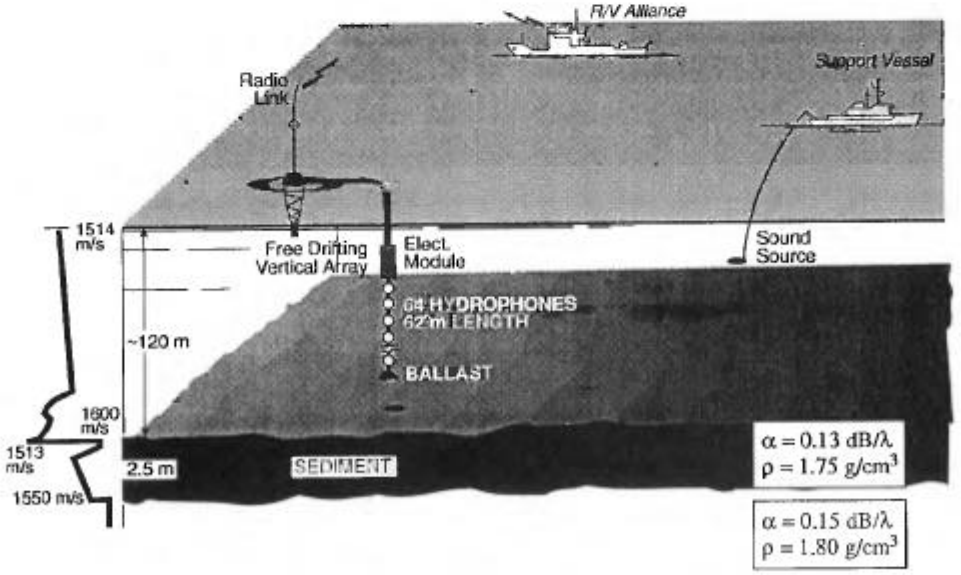

FIG. 1. Environmental/receiving system experimental setup during the North Elba'89 sea trial.

used to generate the normal-mode functions and to compute the modal attenuation coefficients. For simulation purpose, only 32 hydrophones out of the 64-element array are used. The spacing is constant and equal to 2 m. The vertical array spans the water column from 40- to 102-m depth. The sound source is located 10 km away from the receiver and its depth is 60 m. The source signal is a continuous wave tone at 323.7 Hz. Different signal-to-noise ratio (SNR) sequences were generated by varying the source power $\sigma_b^2 = E[b_n^2]$ according to the definition

$$\mathrm{SNR}_{\mathrm{dB}} = 10 \log_{10} \frac{\sigma_b^2 |\mathbf{p}(\theta_T)|^2}{\sigma_\epsilon^2}, \tag{9}$$

where σ_ϵ^2 is the noise power. The number of time snapshots was $N = 50$. The range-depth search variation was from 0 to 20 km in range and from 0 to 120 m in depth. Figure 2 shows the detection ratio (difference in dB between the maximum and the highest sidelobe in the range/depth ambiguity surface) as a function of SNR for three matched-field processors: the conventional matched-field (CMF), the generalized minimum variance (MV),[10] and the mode subspace (MS). The performance of the MV and MS processors clearly stand at 9 and 11 dB, respectively, above that of the CMF processor. The MS processor gave an improvement of approximately 2 dB over the MV processor for almost all the SNR's. This result has to be linked to the range-depth localization errors that are respectively given by

$$R_{\mathrm{ERR}}(\%) = \frac{|\hat{r} - r_T|}{R} \text{ and } D_{\mathrm{ERR}}(\%) = \frac{|\hat{z} - z_T|}{Z}, \tag{10}$$

where R is 20 km and Z is equal to the water depth. The results are shown in Fig. 3(a) for range and in Fig. 3(b) for depth, where one can note that the best performance was achieved by the MS and CMF processors while the MV processor gave a slightly poorer result.

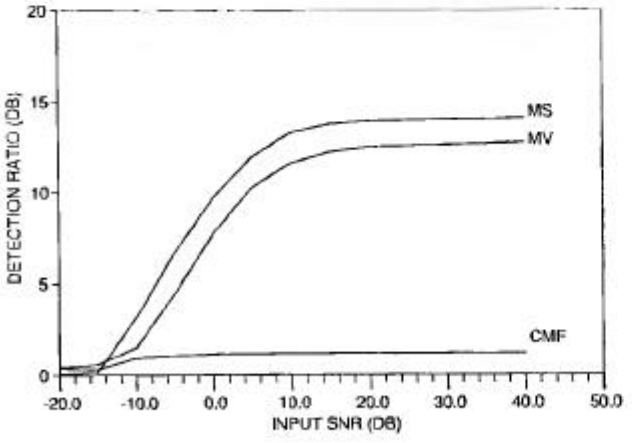

FIG. 2. Narrow-band case: detection ratio in dB versus input SNR for conventional matched-field (CMF), generalized minimum variance (MV) and mode subspace (MS) processors: cw at 323.7 Hz, $N = 50$ time snapshots, 32 hydrophones, with 2-m spacing, array depth is 40 m, and the environmental parameters are those of Fig. 1.

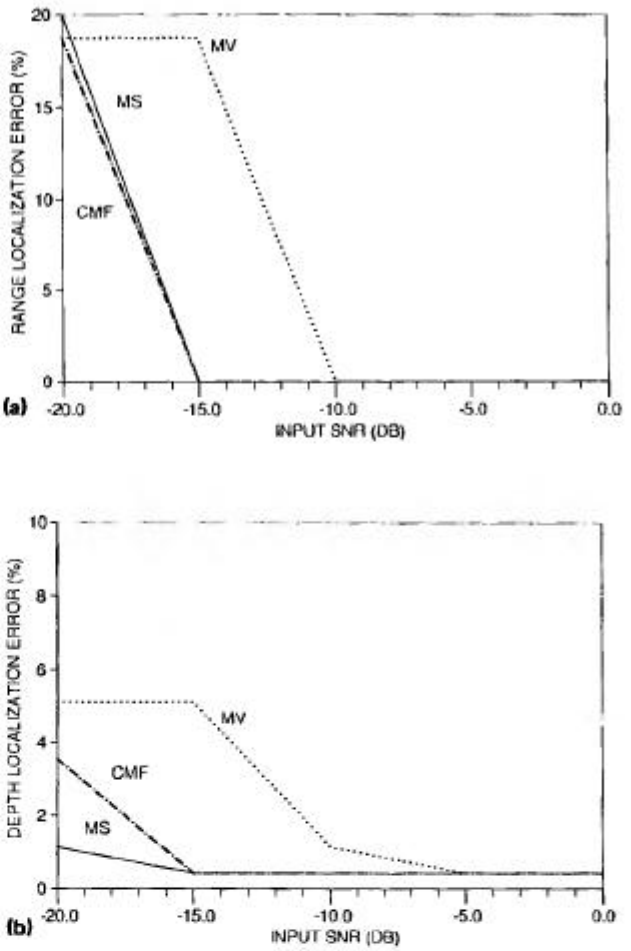

FIG. 3. Source localization errors: (a) range and (b) depth in % versus input SNR in same conditions as in Fig. 2.

The broadband performance was tested by simulating a sound source emitting a linear FM signal in the frequency band 300–350 Hz. A frequency sampling of 1.46 Hz was used, giving rise to 34 range-depth ambiguity surfaces obtained over the source frequency band. These surfaces were frequency averaged according to (8) with $\beta_k = 1$ for the MS, MV,[10] and CMF processors and the results are shown in Fig. 4. Comparison with Fig. 2 shows that the performance of the three processors has been improved by approximately 2 dB while their relative performance is unchanged, except for the MV processor that reaches the MS processor for SNR = 40 dB. The range-depth estimation performance (not shown) has been improved in the broadband case when compared to the results obtained in narrow band. In fact, all three processors gave the correct source location for all the SNR variation. In other words, the significant improvement due to broadband processing was the stabilization of the source location estimate at low SNR.

III. EXPERIMENTAL RESULTS

The system/environment scenario is shown in Fig. 1. Data from the 64 unequally spaced sensors of the vertical array were acquired and processed. The sampling rate was

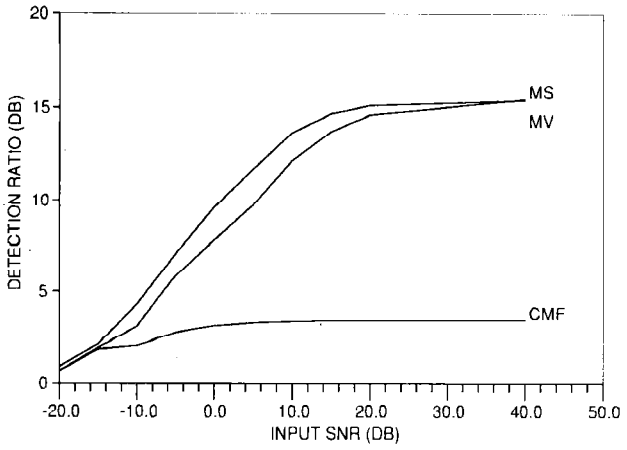

FIG. 4. Broadband case: detection ratio in dB versus input SNR for conventional matched-field (CMF), generalized minimum variance (MV) and mode subspace (MS) processors. Linear FM signal in the band 300–350 Hz, $N = 50$ time snapshots, 32 hydrophones with 2-m spacing, array depth is 40 m and the environmental parameters are those of Fig. 1.

$f_s = 3000$ Hz and the recording time $T_r = 0.68$ s, which corresponds to a block size $2K = 2048$ and $N = 1$. The transient signals were a series of exponentially damped sinusoids with the same center frequency $f_c = 250$ Hz and different durations. The results shown here were obtained for three signal durations: 25 ms (B1), 100 ms (B2), and 500 ms (B3). Signal B3 behaves as a narrow band because its bandwidth (2 Hz) corresponds to, approximately, our frequency interval of 1.46 Hz. The other two signals, B1 and B2, have bandwidths of 40 and 15 Hz, containing approximately 26 and 10 frequency bins, respectively. The experimental input signal-to-noise ratio was estimated by the ratio between the mean power received on the signal frequency band and the (assumed noise) power received outside this band. The broadband mode subspace processor has been used throughout and compared, for reference, with the broadband conventional matched-field processor. The maximum amplitude of each ambiguity surface was used for normalization, and its range-depth coordinates were compared to the expected true source coordinates; the range-depth errors were calculated according to (10). In order to give an idea of the sidelobe aspect of the surface, the highest sidelobe was found, and the

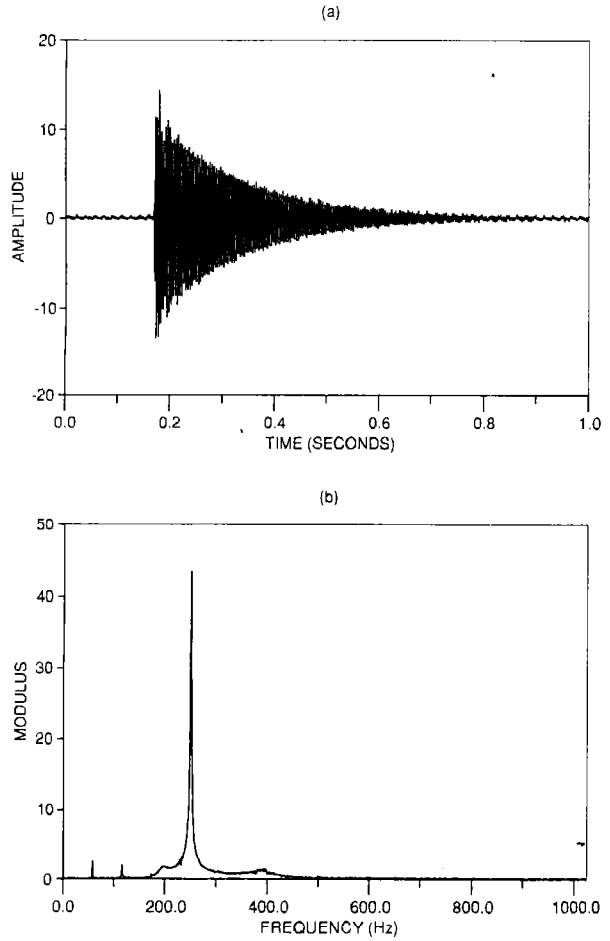

FIG. 5. (a) Time waveform and (b) power spectrum of the received direct path source pulse signal code B3, transmitted with an HX90G sound source, duration 500 ms, center frequency 250 Hz, bandwidth 2 Hz.

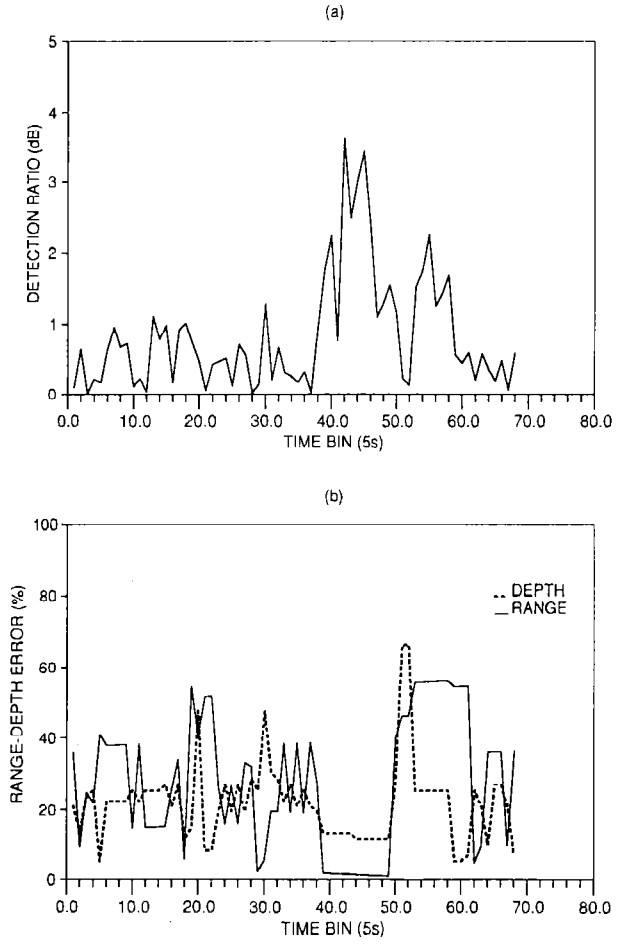

FIG. 6. Experimental data results in the narrow-band case code B3 with the mode subspace processor, $f = 249$ Hz. (a) Detection ratio (dB) versus time bin (5 s) and (b) source localization range and depth errors in % for a depth variation from 0 to 122 m and a range variation from 0 to 20 km. True source location is in the 8.3-km range and 70-m depth.

detection ratio, defined as the difference in dB between the main peak and the highest sidelobe, was calculated. This was repeated for all the pulses during each run and the results are displayed as a function of time snapshot. It should also be noted that during the experiment the depth sensor placed on the sound source was not working properly and the assumed source depth z_T was in fact roughly estimated from the cable scope.

A. Narrow-band transient signals

A direct path measurement of the 500-ms-long transient pulse code B3 is shown in Fig. 5. This signal was transmitted with a repetition rate of 5 s. Each pulse was processed for the frequency of 249 Hz, which was the frequency showing the maximum energy at the receiver. This was repeated for all the pulses during the run for approximately 6 min, giving rise to 68 time pings. The mean signal-to-noise ratio at the array has been estimated to approximately 25 dB. The water depth was taken to be 122 m for that run. The results obtained using the mode-subspace method are shown in Fig. 6(a) for the detection ratio and in Fig. 6(b) for the range-depth estimation error. Figure 6(a) shows a detection ratio that is relatively low ($\leqslant$1 dB), except for a time interval of about 1 min between time bins 38 and 50, where it increases to almost 4 dB. The range-depth error curves, shown in Fig. 6(b), attain high error rates up to 60% except for a short interval between time bins 39 and 49, where the range estimate is correct and the depth estimate shows an error of about 11%. This depth error corresponds to a source depth estimate of 56 m while the true source depth was assumed equal to 70 m; the fact that depth errors of the same order were found in most of the runs [e.g., Figs. 10(b) and 13(b)] and due to the source depth sensor problems experienced during the experiment, leads us to the hypothesis that the source depth estimate might be correct. As an example a series of range-depth contour plots are shown in Fig. 7 for time bins 39 to 48. The estimated location is obtained directly from the figure and is in the 8-km range and approximately 56-m depth.

B. Broadband transient signals

A direct path measurement of the pulse codes B1 and B2 is shown in Figs. 8 and 9, respectively. Note that there is an

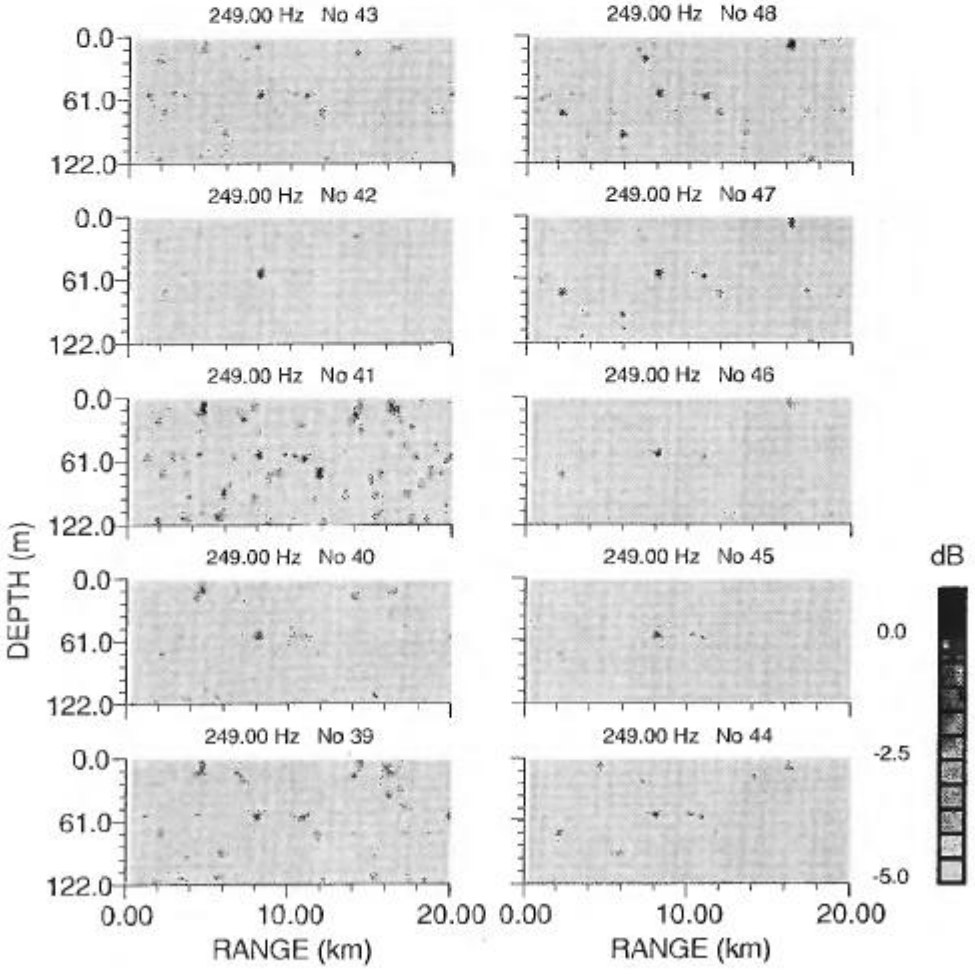

FIG. 7. Range-depth ambiguity surfaces obtained from real data code B3 with the mode subspace processor, time bin from 39 to 48, interval 5 s. Estimated source location is in the 8-km range and 56-m depth.

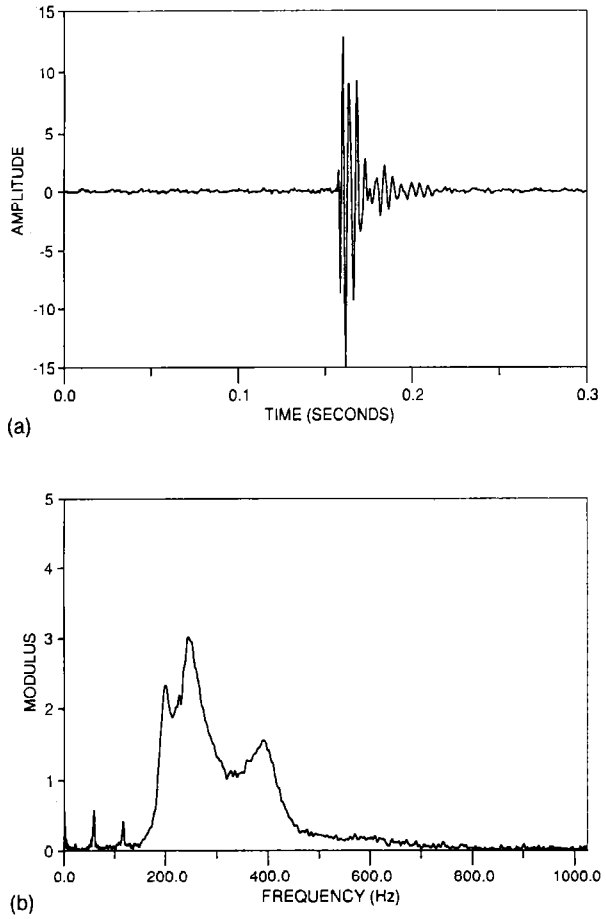

FIG. 8. (a) Time waveform and (b) power spectrum of the received direct path source pulse signal code B1, transmitted with an HX90G sound source, duration 25 ms, center frequency 250 Hz, bandwidth 40 Hz.

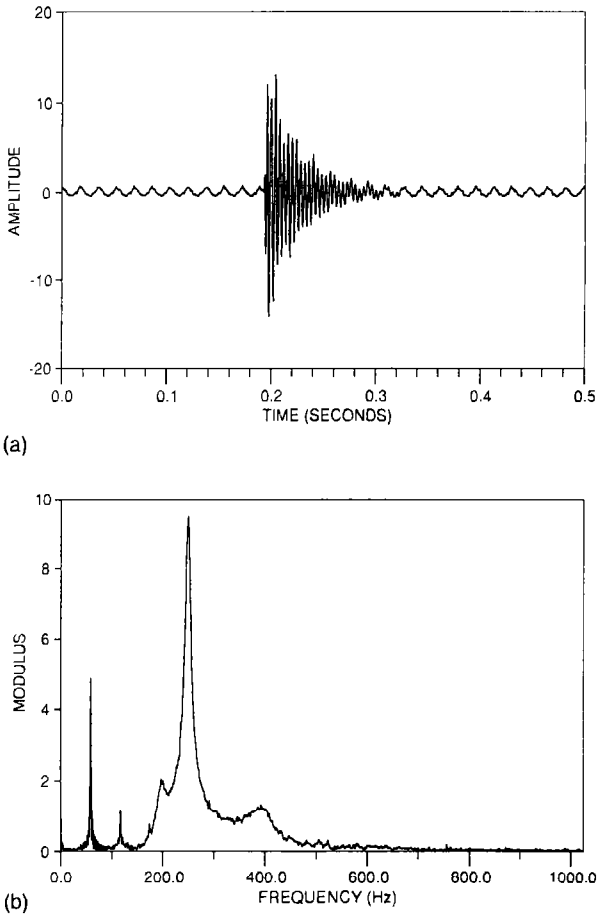

FIG. 9. (a) Time waveform and (b) power spectrum of the received direct path source pulse signal code B2, transmitted with an HX90G sound source, duration 100 ms, center frequency 250 Hz, bandwidth 15 Hz.

ac power supply interference pickup at 60 and 120 Hz that is due to the direct path recording system and has no influence on the results as the received data has been 200–800 Hz band-pass filtered prior to any matched-field processing. A signal-to-noise ratio of approximately 10 dB for B1 and 15 dB for B2 has been measured at the hydrophone input. The frequency bands that have been used for processing were from 235 to 265 Hz for B1 and from 245 to 255 Hz for B2. A range-depth surface was obtained for each frequency bin and then was averaged over the band. Three types of weighting coefficients [β_k in (8)] were used for the frequency averaging: (1) proportional to the source power spectrum, (2) pro-

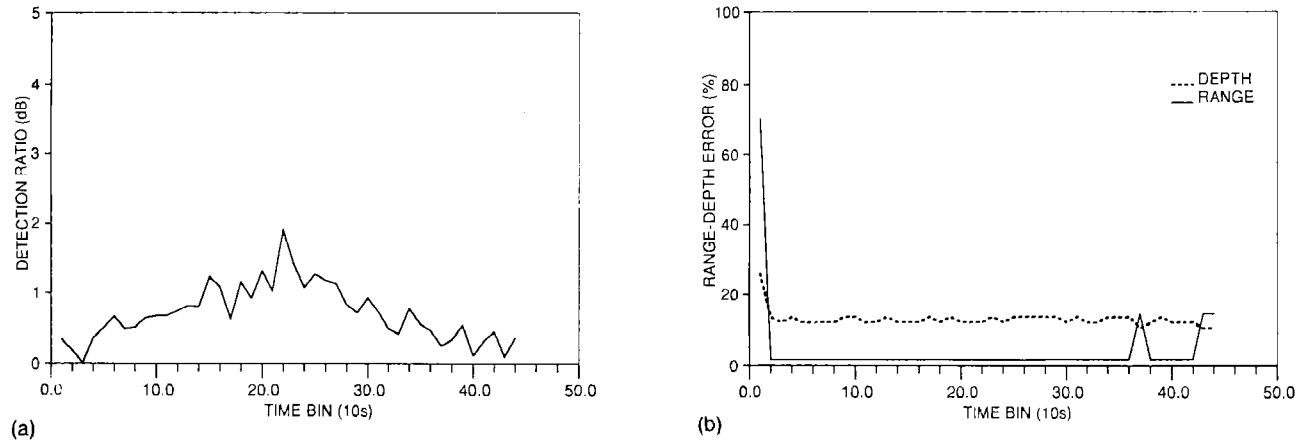

FIG. 10. Experimental data results in the broadband case code B2 with the mode subspace processor, $f = 244$–256 Hz. (a) Detection ratio (dB) versus time bin (10 s) and (b) source localization range and depth errors in % for a depth variation from 0 to 119 m and a range variation from 0 to 20 km. True source location is in the 3.7-km range and 70-m depth.

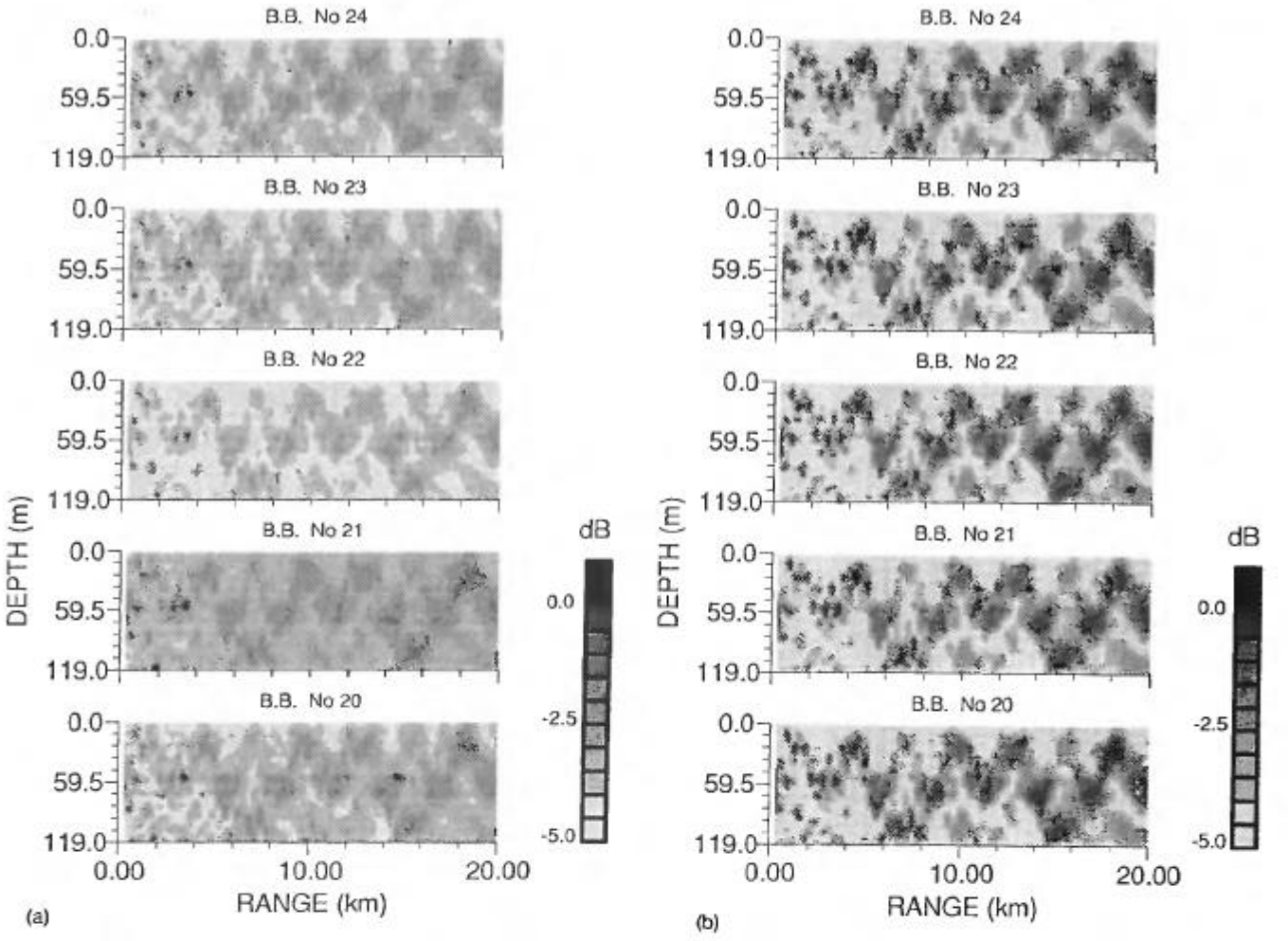

FIG. 11. Broadband range-depth ambiguity surfaces obtained from real data code B2 in the frequency band 244–256 Hz for time bins 20 to 24 at a 10-s interval: (a) with the mode subspace processor and (b) with the conventional matched-field processor.

portional to the received signal power spectrum, and (3) no weighting, i.e., $\{\beta_k = 1; k = k_1, \ldots, k_2\}$. The results were similar for the source and received signal power spectrum weighting coefficients while a slight degradation was noticed in the case where no weighting was used. Figure 10 shows the results obtained for signal B2 with source power spectrum weighting and for a total run duration of 7 min corresponding to 44 time bins at 10 s interval. From Fig. 10a it can be noticed that the detection ratio is oscillating between 0.5 and 2 dB. Figure 10(b) shows that the true source range of 3.7 km has been successfully estimated and the true source depth of 70 m has a constant error of about 11% as in the case of signal B3. It should be noticed that the localization is stable throughout the 7-min run. This can be visualized by looking at Fig. 11 that shows a sequence of five range-depth contour plots for time bins from 20 to 24 obtained in Fig. 11(a) with the MS processor and in Fig. 11(b) with the CMF processor. Comparing Fig. 11(a) and (b) it can be noticed that the spatial field structure is the same for both processors with, however, a much higher peak-to-sidelobe rejection in 11(a), using the MS processor, than in 11b using the CMF processor. In Fig. 11(b) there is a very large sidelobe ambiguity and the source is erroneously located at the 1-km range and 25-m depth. In order to be able to access the relative performance of the broadband versus narrow-band processing, a single frequency line (249 Hz) has been extracted from the broadband data and processed. The results obtained with the MS processor are shown in Fig. 12 and indicate that although at some moments a high detection ratio is obtained [Fig. 12(a)] it does not correspond to any accurate and stable source location estimate [Fig. 12(b)]. The running of the CMF processor in the same example gave similar results in terms of source localization instability with, however, a much lower detection ratio. Other single frequencies within the source signal frequency band gave similar results. It can be concluded that the broadband processing of transient signals, as compared to the narrow band, although it gave no improvement of the detection ratio, it increased the stability of the source location estimate as was predicted by the simulations.

Figure 13 shows the results obtained with signal code B1 for a total time duration of 16 min corresponding to 48 time bins at 20-s intervals. Source power spectrum weighting was used for the frequency averaging over the received source signal frequency band. In this run the power of the source was varied; it was set to full power during the first 7 min

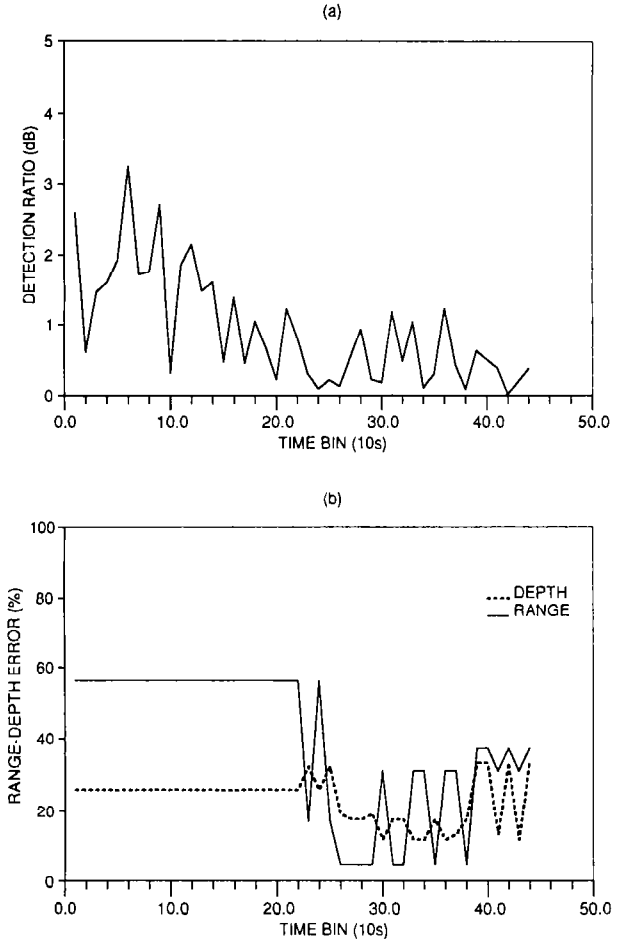

FIG. 12. Narrow-band processing of code B2 with the mode subspace processor, $f = 249$ Hz. (a) Detection ratio (dB) versus time bin (10 s) and (b) source localization range and depth errors in % for a depth variation from 0 to 119 m and a range variation from 0 to 20 km. True source location is in the 3.7-km range and 70-m depth.

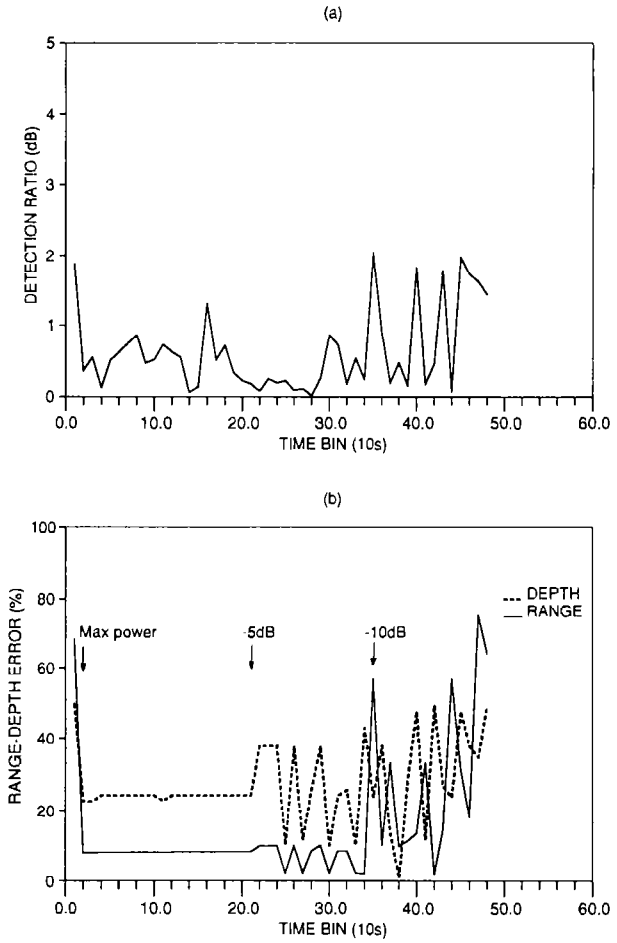

FIG. 13. Experimental data results in the broadband case code B1 with the mode subspace processor, $f = 235$–265 Hz. (a) Detection ratio (dB) versus time bin (20 s) and (b) source localization range and depth errors in % for a depth variation from 0 to 119 m and a range variation from 0 to 20 km. From bin 1 to 21 at max source power, between bin 21 and 35 at max power—5 dB and from bin 35 to the end at max power—10 dB. True source location is in the 3.9-km range and 70-m depth.

(until bin 21), then decreased 5 dB for the following 5 min (bin 21 to 35), and then decreased again by 5 dB for the remaining time. These time intervals are indicated by the vertical arrows on Fig. 13. Observation of the range-depth error curves shows that: the localization is stable with 8% error in range and 24% in depth for the first time interval (until bin 21), then it starts to oscillate around the same error values during the second time interval where the source power was decreased by 5 dB (until bin 35), and finally a further decrease on the source power gives unstable source location estimates for the last portion of the run. This behavior is accompanied by a similar evolution on the detection ratio: variable but relatively high detection ratio during the first two time intervals and highly unstable at the end of the run. This example indicates that a decrease of the signal power cannot always be compensated by an increase of the signal bandwidth and continue obtaining stable and accurate localizations. With real data, the probability of model mismatch increases with the increasing of the number of frequencies processed that results on a effect of plateau on the improvement versus signal bandwidth figure. It further shows that the estimated source location is very sensitive to the source power and is not an artifact of the matched-field processor or of the structure of the medium of propagation.

IV. CONCLUSION

Range and depth localization of transient acoustic sources in complex propagation environments is possible by direct estimation of the vector subspace spanned by the normal modes that are significantly excited by the source: the mode subspace. The mode subspace approach has been applied to broadband signals by averaging of the narrow-band estimates of the range-depth ambiguity surfaces over the source signal frequency band. The results obtained with simulated data show that the performance of the mode subspace method is always better than or equal to that of the generalized minimum variance processor that itself performs significantly better than the conventional matched-field processor. When applied to broadband signals the relative performance of the three processors is the same with, however, a significant improvement in the accuracy of the source range-depth estimate for low signal-to-noise ratio.

The processing of experimental broadband transient signals, obtained during the North Elba'89 sea trial in a shallow water area, showed that the broadband mode subspace method could achieve very stable source location estimates with sidelobe rejections up to 2 dB, during longer periods of time than those normally found in previously published studies. Using the broadband conventional matched-field processor on the same real data set gave poor results: no localization could be obtained during the analysis of the whole data set. The minimum variance method was also tested (not shown) with, in some cases, similar results to those obtained with the mode subspace approach. However, severe numerical instability was found due to the need to invert ill-conditioned cross-covariance matrices estimated over a single time snapshot. No environmental/system mismatch study has been done. However, it should be noted that these results were obtained with absolutely no search over any environmental or system parameters. The sound-speed profile and the vertical array position were those measured during the sea trial. No tilt or other array deformation has been tested, and the bottom parameters were those estimated by Jensen[24] in 1974. The encouraging results provided by this new broadband matched-field technique show that reliable range-depth localization of transient signals in shallow water is feasible. Moreover, the observation of the time sequence of range-depth ambiguity surfaces shows that the broadband signal field used by the mode subspace approach is relatively stable in time and highly correlated with the predictions given by a standard normal-mode model. This is, probably, the most important result obtained in this study and leaves great hope for the use of this technique on range-dependent environments and deep water.

ACKNOWLEDGMENTS

Thanks are due to Dr. J. Ianniello and all scientific and engineering staff participating on the sea trial North Elba'89. Thanks are also due to S. Bongi for his help on the plotting software used in this paper.

[1] M. J. Hinich, "Maximum likelihood signal processing for a vertical array," J. Acoust. Soc. Am. **54**, 499–503 (1973).
[2] H. P. Bucker, "Use of calculated sound fields and matched-field detection to locate sound sources in shallow water," J. Acoust. Soc. Am. **59**, 368–373 (1976).
[3] R. Klemm, "Range and depth estimation by line arrays in shallow water," Signal Process. **3**, 333–344 (1981).
[4] E. C. Shang, "Source depth estimation in waveguides," J. Acoust. Soc. Am. **77**, 1413–1418 (1985).
[5] E. C. Shang, C. S. Clay, and Y. Y. Wang, "Passive harmonic source ranging in waveguides by using mode filter," J. Acoust. Soc. Am. **78**, 172–175 (1985).
[6] M. B. Porter, R. L. Dicus, and R. G. Fizell, "Simulations of matched-field processing in a deep-water Pacific environment," IEEE J. Ocean. Eng. **OE-12**(1), 173–181 (1987).
[7] T. C. Yang, "A method of range and depth estimation by modal decomposition," J. Acoust. Soc. Am. **82**, 1736–1745 (1987).
[8] G. R. Wilson, R. A. Koch, and P. J. Vidmar, "Matched mode localization," J. Acoust. Soc. Am. **84**, 310–320 (1988).
[9] D. R. DelBalzo, C. Feuillade, and M. M. Rowe, "Effects of water depth mismatch on matched-field localization in shallow water," J. Acoust. Soc. Am. **83**, 2180–2185 (1988).
[10] A. B. Baggeroer, W. A. Kuperman, and H. Schmidt, "Matched-field processing: source localization in correlated noise as an optimum parameter estimation problem," J. Acoust. Soc. Am. **83**, 571–587 (1988).
[11] R. M. Hamson and R. M. Heitmeyer, "Environmental and system effects on source localization in shallow water by the matched-field processing of a vertical array," J. Acoust. Soc. Am. **86**, 1950–1959 (1989).
[12] C. Feuillade, D. R. DelBalzo, and M. M. Rowe, "Environmental mismatch in shallow water matched-field processing: Geoacoustic parameter variability," J. Acoust. Soc. Am. **85**, 2354–2364 (1989).
[13] D. F. Gingras, "Methods for predicting the sensitivity of matched-field processors to mismatch," J. Acoust. Soc. Am. **86**, 1940–1949 (1989).
[14] G. B. Smith, C. Feuillade, D. R. DelBalzo, and C. L. Byrne, "A nonlinear matched-field processor for detection and localization of a quiet source in a noisy shallow water environment", J. Acoust. Soc. Am. **85**, 1158–1166 (1989).
[15] S. M. Jesus, "Normal-mode matching localization in shallow water: environmental and system effects," J. Acoust. Soc. Am. **90**, 2034–2041 (1991).
[16] J. M. Ozard, "Matched field processing in shallow water for range, depth and bearing determination: Results of experiment and simulation," J. Acoust. Soc. Am. **86**, 744–753 (1989).
[17] C. Feuillade, W. A. Kinney, and D. R. DelBalzo, "Shallow water matched-field localization off Panama City, Florida," J. Acoust. Soc. Am. **88**, 423–433 (1990).
[18] J. Q. D. Tran and W. S. Hodgkiss, "Matched-field processing of 200-Hz continuous wave (cw) signals," J. Acoust. Soc. Am. **89**, 745–755 (1991).
[19] W. S. Hodgkiss and R. K. Brienzo, "Broadband source detection and range-depth localization via full-wavefield (matched-field) processing," in *Proceedings of ICASSP*, Albuquerque, New Mexico, 1990) (IEEE, Piscataway, NJ, 1990), pp. 2743–2746.
[20] I. Tolstoy and C. S. Clay, *Ocean Acoustics* (McGraw-Hill, New York, 1966), Chap. 3–7, pp. 81–85.
[21] T. W. Anderson, *An Introduction to Multivariate Statistical Analysis* (Wiley, New York, 1984), 2nd ed., Chap. 14.2, p. 552.
[22] R. O. Schmidt, "A signal subspace approach to multiple emmiter location and spectral estimation," Ph.D. dissertation, Stanford University (1982).
[23] G. Bienvenu, "Influence of the spatial coherence of the background noise on high resolution passive methods," in *Proceedings of the ICASSP*, Washington, DC, 1979 (IEEE, Piscataway, NJ, 1979), pp. 306–309.
[24] F. B. Jensen, "Comparison of transmission loss data for different shallow water areas with theoretical results provided by a three-fluid normal-mode propagation model," La Spezia, Italy, SACLANT Undersea Research Centre, SACLANTCEN CP-14 (1974).
[25] F. B. Jensen and M. C. Ferla, "SNAP: The SACLANTCEN normal-mode acoustic propagation model," La Spezia, Italy, SACLANT Undersea Research Centre, SACLANTCEN SM-121 (1979).